Composites Part B 101 (2016) 1–13

Contents lists available at ScienceDirect

Composites Part B

journal homepage: www.elsevier.com/locate/compositesb

Self-healing capability of large-scale engineered cementitious composites beams

Suleyman Bahadir Keskin [a], Ozlem Kasap Keskin [a], Ozgur Anil [b, *], Mustafa Şahmaran [b], Ahmed Alyousif [c], Mohamed Lachemi [c], Lamya Amleh [c], Ashraf F. Ashour [d]

[a] Department of Civil Engineering, Mugla Sitki Kocman University, Mugla, Turkey
[b] Department of Civil Engineering, Gazi University, Ankara, Turkey
[c] Department of Civil Engineering, Ryerson University, Toronto, ON, Canada
[d] School of Engineering, Bradford University, West Yorkshire, UK

ARTICLE INFO

Article history:
Received 7 March 2016
Received in revised form
8 June 2016
Accepted 28 June 2016
Available online 1 July 2016

Keywords:
Smart materials
Strength
Damage mechanics
Mechanical testing

ABSTRACT

Engineered Cementitious Composites (ECC) is a material which possesses advanced self-healing properties. Although the self-healing performance of ECC has been revealed in numerous studies, only small-scale, laboratory-size specimens have been used to assess it under fixed laboratory conditions and curing techniques. In order to evaluate the effect of intrinsic self-healing ability of ECC on the properties of structural-size, large-scale reinforced-beam members, specimens with four different shear span to effective depth (a/d) ratios, ranging from 1 to 4, were prepared to evaluate the effects of shear and flexural deformation. To ensure a realistic assessment, beams were cured using wet burlap, similar to on-site curing. Each beam was tested for mechanical properties including load-carrying capacity, deflection capacity, ductility ratio, yield stiffness, energy absorption capacity, and the influence of self-healing, by comparing types of failure and cracking. Self-healed test beams showed higher strength, energy absorption capacity and ductility ratio than damaged test beams. In test beams with an a/d ratio of 4 in which flexural behavior was prominent, self-healing application was highly successful; the strength, energy absorption capacity and ductility ratios of these beams achieved the level of undamaged beams. In addition, flexural cracks healed better, helping recover the properties of beams with predominantly flexural cracks rather than shear cracks.

1. Introduction

Concrete is the most widely used construction material in the world. However, its brittle behavior and low tensile strength affect not only mechanical performance, but also influence durability through cracking, limiting the service life of reinforced concrete structures and requiring maintenance and repair to ensure serviceability. Repairing concrete structures is not an easy task; it is expensive and requires specialized expertise and materials. For example, approximately $5.2 billion is spent each year to maintain existing bridges in the United States [1]; the estimated budget for reconstructing them is between $20 billion and $200 billion [2,3]. The situation is similar around the globe; 45% of the construction and building budget in the United Kingdom is spent on repair and maintenance applications [4]. Annual maintenance and repair costs are also substantial for the European Union countries, with actual spending of around $1 billion for the maintenance of bridges, with an estimated $20 billion for all infrastructure types [5]. However, over the last two decades, the self-healing capabilities of cementitious materials have become an attractive solution for reducing maintenance and repair costs; materials with self-healing ability have the potential of recovering their properties after cracking. Studies have shown that the mechanical performance and transport properties of these kinds of materials can be re-attained, and that even after substantial damage, the self-healing mechanism can help the material reach its initial properties and behave as if it had never been subjected to damage. Numerous self-healing techniques have emerged, some requiring unconventional ingredients such as hollow fibers, encapsulation with chemicals, bacteria, expansive agents and shape memory materials [6,7]. One mechanism is autogenous or intrinsic self-healing, which involves the plugging of cracks with materials incorporated into the cementitious

* Corresponding author.
E-mail address: oanil@gazi.edu.tr (O. Anil).

http://dx.doi.org/10.1016/j.compositesb.2016.06.073
1359-8368/

composite, without any additional process or agent. It has been reported that the mechanism of intrinsic self-healing is a consequence of the chemical, mechanical and physical closure of existing cracks. This kind of self-healing is generally attributed to the hydration of previously unhydrated cementitious material, calcite formation, expansion of concrete in the crack flanks, crystallization, closing of cracks by solid matter in the water, and closing of cracks by spalling of loose concrete particles resulting from cracking [8]. Self-healing should be taken into account when specifying tolerable crack widths. Jacobsen et al. [8], Reinhardt and Joss [9], Sahmaran and Yaman [10], Edvardsen [11], Aldea et al. [12] and Clear [13] have proposed maximum crack widths of 5–10 μm, 100 μm, 200 μm, 205 μm and 300 μm, respectively, for a crack to seal itself completely. Overall, the most serious challenge for complete healing is tolerable crack width. Since conventional concrete has the tendency to deform in a brittle manner under mechanical loading, attaining such small crack widths is a major concern. However, the situation is different for ECC, which deforms in a ductile manner and is characterized by tensile strain hardening and flexural deflection hardening properties. These are the result of self-controlled multiple tight cracks that remain under 100 μm, and are likely to promote intrinsic self-healing ability. In addition, ECC material contains large amounts of supplementary cementitious materials, which also make it possible for unhydrated cementitious material to exist in the structure, allowing further hydrates to fill up the microcracks. ECC is a prominent intrinsic self-healing construction material, well-documented in the literature [7].

However, studies focusing on the influence of self-healing on a structural scale are limited. One study into reinforced large-scale structural members was performed by Tran Diep et al. [14], in which four-point bending tests were performed on relatively large beams (125 mm × 200 mm × 2000 mm) containing encapsulated epoxy. Dry [15] also investigated the possibility of obtaining autonomous crack healing in a real-scale concrete bridge deck (76 mm × 1220 mm × 6096 mm) using adhesive-filled glass tubes. However, no study has been conducted into the self-healing ability of ECC on a structural scale. Numerous studies into ECC's self-healing capability are restricted by their use of small specimens with no reinforcement and single-type microcracks formed by tensile or flexural loading. However, the authors believe that a study into the effects of self-healing behavior of large-scale ECC members on important structural parameters such as strength, stiffness, ductility, energy absorption capacity and failure mechanism should be conducted to promote the use of such a successful self-healing material in real structures. Although ECC is a perfect material in terms of ductility and self-healing as determined under laboratory conditions, yet studies on large scale ECC members are quite limited. This deprives construction industry from the benefits of structural use of ECC. This study may help ECC to be recognized as a structural material and pave the way for a successful use of ECC in structural members. Successful and widespread implementation of ECC may yield more ductile hence more durable structures with smaller construction budgets for repair and retrofitting [16].

In addition, any construction material can be damaged in an earthquake or due to induced stresses originating from durability concerns and unpredicted load conditions. However, ECC has the potential to eliminate the need for repair as a result of its intrinsic self-healing capability. For this reason, beams were subjected to curing for as little as 30 days after being damaged to assess whether self-healing mechanisms of ECC can replace repair, which would be a great benefit for the construction industry. ECC is composite material type, and theoretical modeling of composite structures using this type of materials should be investigated [17–22].

This paper outlines an experimental investigation into the self-healing performance of large-scale reinforced ECC beam specimens. The main variables investigated were the shear span to effective depth (a/d) ratios of the reinforced ECC beams. This was mainly intended to reflect real-life cracking behavior of reinforced composites; crack formation is possible due to both shearing and bending effects. For this purpose, four different a/d ratios were chosen, ranging between 1 and 4. To examine the self-healing performance of reinforced ECC beams, twelve beam specimens, including three beams from each test group, were tested under four-point bending loading. The study investigated the effect of self-healing performance on structural characteristics such as strength, stiffness, ductility ratio, energy absorption capacity and failure mechanisms of test members and the way they are influenced by self-healing.

2. Experimental program

2.1. Test specimens and material properties

To evaluate self-healing characteristics of large-scale reinforced ECC beams, specimens with different shear span (a) to effective depth (d) ratios were tested under the four-point bending test. The a/d ratios of reinforced ECC beam specimens ranged from 1 to 4 so that shearing effects could be observed. According to Fig. 1 [23], which describes the changes in failure modes of reinforced concrete beams with respect to a/d ratio, as a/d ratio decreased, the possibility of shear failure increased. Therefore, a low ratio between 1 and 3 was selected to promote shear failure and monitor the behavior of test specimens under the influence of shear forces. Additionally, a high a/d ratio of 4 was used to obtain a different failure mode, which was expected to be a combination of shear and flexural failure mechanisms.

All test beams were produced with the same amount of reinforcement, obtained from the same supplier throughout the study. Geometric dimensions and steel reinforcement details of test specimens are shown in Fig. 2. Main longitudinal tensile reinforcements of 2φ16 were used for all a/d ratios. The yield strength (f_{sy}), ultimate strength (f_{su}) and elastic modulus (E) of φ16 ribbed steel bars were determined as 520 MPa, 625 MPa and 205 GPa, respectively. Only a small amount of shear reinforcement was placed at the support regions to prevent local failure at those points. No additional shear reinforcement was applied along the beam length. Shear reinforcing bars had a 10 mm diameter, with 428 MPa yield strength, 535 MPa ultimate strength and 198 GPa elastic modulus. The main test specimen parameters are presented in Table 1.

Three groups of reinforced beam specimens with four a/d ratios were produced and tested for the study. The main aim was to examine the effects of self-healing performance on major residual structural parameters such as load-deformation behavior, strength, stiffness, ductility ratio and energy absorption capacity. The effects of the change in a/d ratio on self-healing performance of beams were also examined. In the nomenclature of the test members provided in Table 1, the first three characters show the a/d ratio, while the last three characters designate the test age: 28 or 58 days (28D or 58D). "V" in the beam notations means that the beam is virgin, i.e. it is the reference value. "PL" refers to the fact that a preloading up to 50% of the maximum load-carrying capacity was applied on the beam specimens. "SH", which appears in the last four test members, means that the self-healing process was applied on those beams.

In the first test group, one reference beam was tested until failure for each a/d ratio at the end of 28 days of standard curing to determine load-carrying capacities (specimens 1, 2, 3 and 4). Two sets of experiments were performed on specimens 5, 6, 7 and 8 (second test group). At 28 days, those specimens were preloaded up

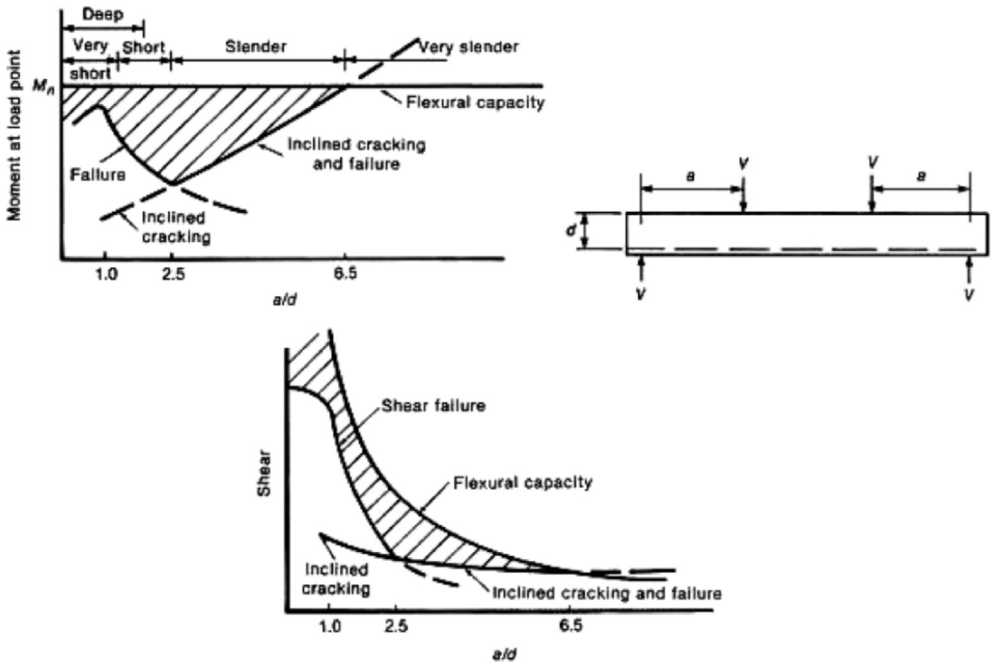

Fig. 1. Variation of failure modes, and shear and moment capacities of RC beams against a/d ratio [23].

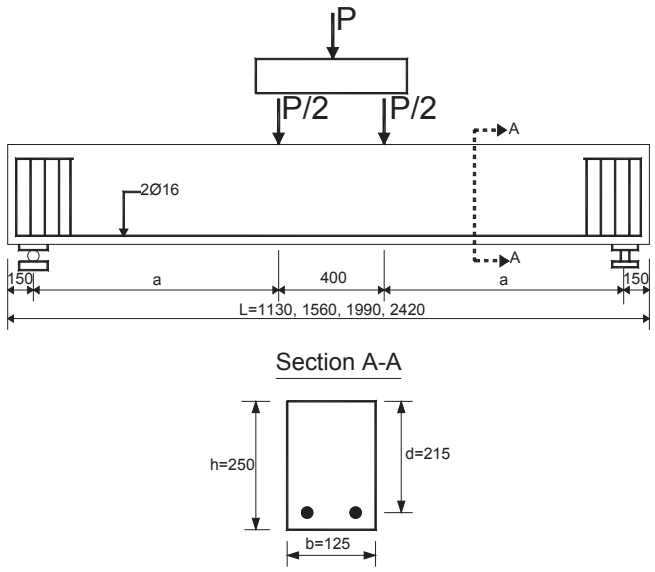

Fig. 2. Reinforcement details of the specimens.

to 50% of their maximum load-carrying capacities, as determined from the reference beams. After removing the load, the damaged beam specimens were reloaded immediately up to failure without considering the effect of self-healing. Results obtained from the second group test specimens showed the behavior of damaged beams under loading. Beams belonging to the third group (specimens 9, 10, 11 and 12) were tested in the same two stages as the second group. At 28 days, all beams were preloaded up to 50% of their maximum load-carrying capacities, then the loads were removed immediately. After removal of the load, the damaged beams were kept in laboratory conditions at 23 ± 1 °C, covered in wet burlap which was rewetted three times a week. This curing condition was chosen to imitate in situ conditions, as it is common practice to cover structural members in wet burlap, and it is also possible to apply a similar curing method in real structures. The necessary moisture for self-healing of damaged beam specimens was supplied solely by the wet burlap, which was covered with plastic sheets to prevent moisture loss during curing. Fig. 3 shows the curing conditions of specimens subjected to the self-healing process. The damaged beam specimens were left for self-healing to develop for an additional 30 days. At 58 days after casting, beams 9, 10, 11 and 12 were loaded up to failure to evaluate self-

Table 1
Values of main parameters of test specimens.

Spec. #		Beam name	Beam length(mm)	a/d ratio	Remark
1	First Group	AD1_V_28D	1130	1	Reference specimens, Loaded up to failure after 28 days
2		AD2_V_28D	1560	2	
3		AD3_V_28D	1990	3	
4		AD4_V_28D	2420	4	
5	Second Group	AD1_PL_28D	1130	1	First Step (Preload PL): Loaded upto 50% level of ultimate capacity after 28 days and unloaded.
6		AD2_PL_28D	1560	2	Second Step (Reload RL): After the first step, the same damaged specimen loaded up to failure.
7		AD3_PL_28D	1990	3	
8		AD4_PL_28D	2420	4	
9	Third Group	AD1_SH_58D	1130	1	First Step (Preload PL): Loaded up to 50% level of ultimate capacity after 28 days and unloaded.
10		AD2_SH_58D	1560	2	Second Step: Applied the self-healing process up to 30 days.
11		AD3_SH_58D	1990	3	Third Step (Reload RL): After the self-healing process the same damaged specimen loaded up to failure.
12		AD4_SH_58D	2420	4	

Fig. 3. Specimens covered with wet burlap.

healing performance compared to the other two test series.

ECC mixtures used for all test specimens were produced with identical proportions of the same ingredients to ensure similar properties. ECC has ingredients which are similar to those of typical fiber-reinforced concrete; CEM I 42.5 type cement (similar to ASTM Type I), Class F fly ash, aggregate, water, fibers, and a high-range water-reducing admixture (HRWRA) were employed for ECC production in this study. Mixture proportions are presented in Table 2. The ECC mixture had a water to cementitious material ratio (W/CM) of 0.27 and a fly ash to Portland cement ratio (FA/PC) of 2.2, by mass. In order to obtain multiple microcracking and consequently strain-hardening behavior, it is necessary to minimize matrix fracture toughness. For this purpose, only fine aggregates were used for ECC production; silica sand with a maximum particle size of 1 mm was incorporated into the ECC mixtures used for the production of the beams. Straight poly-vinyl-alcohol (PVA) fibers with a tensile strength of 1610 MPa, an average diameter of 39 μm, and an average length of 8 mm as provided by the manufacturer were used in the mixture as 2% of the total volume. HRWRA was added until the desired fresh ECC characteristics were visually observed, as described in [24]. Compressive strength of the ECC mixtures was determined as the average of six Ø100 × 200 mm cylinder specimens. Flexural strength and deflection were determined by testing six 400 × 100 × 75 mm beam specimens. Four-point bending tests were performed at a loading rate of 0.005 mm/s, using a universal testing machine for the flexural parameters. As shown in Table 2, 28-daycompressive and flexural strengths were 46.1 MPa and 7.41 MPa, respectively. Besides, mid-span beam deflection at 28-days was measured as 4.52 mm.

Table 2
Mixture proportions and basic mechanical properties.

Ingredients, (kg/m^3)	
Portland cement	375
Fly ash	823
Water	318
Silica sand	435
PVA fiber	26.0
HRWRA	3
Mechanical properties (28-day)	
Compressive strength (MPa)	46.1
Flexural strength (MPa)	7.41
Flexural deformation (mm)	4.52

2.2. Test setup and instrumentation

A four-point bending test setup was used to evaluate the behavior and self-healing performance of reinforced ECC beams with different a/d ratios under flexural loading. Mid-span beam deflection, crack width in both shear spans and strain in tensile reinforcements were recorded at each load increment. The test setup and locations of LVDTs are shown in Fig. 4.

To plot the load-deflection curves of the ECC beams, the vertical deflection values recorded at the mid-span of the maximum moment region and three points on both symmetrical sides of the beams were considered. Strength, stiffness, ductility ratio and energy absorption capacity for the virgin (group 1), damaged (group 2) and self-healed (group 3) beams were determined from the load-deflection curves. For strain measurements of tensile reinforcement, strain gauges were attached at the maximum moment regions of both reinforcing steel bars before casting.

Shear deformation resulting from shear cracks was calculated using three LVDTs, symmetrically placed on the left and right shear spans of the beams. These were, in turn, used to calculate shear deformation percentage in total mid-span deflections (Fig. 4). As the distance of vertical shear deflections to mid-span was equal for the left and right spans, an average of the results from both sides of each beam was recorded. Fig. 5 provides the approach used for this calculation, along with the strain geometry. Vertical shear deflection, the component of LVDT measurements recorded from left and right shear spans, was calculated using Eqs (1)–(4). Definitions of notations used in Eqs. (1)–(4) are also shown in Fig. 5.

$$\alpha = acr\tan\left(\frac{y_a}{x_a}\right) = acr\tan\left(\frac{\left(\frac{l'_1-l'_2}{2}\right)\sin(\theta)}{\left(\frac{l'_1+l'_2}{2}\right)\cos(\theta)}\right) = \arctan\left(\frac{l'_1-l'_2}{l'_1+l'_2}\right)\tan(\theta) = acr\tan\left(\frac{l'_1-l'_2}{l'_1+l'_2}(h/w)\right) = acr\tan\left(\frac{\varepsilon_1-\varepsilon_2}{2+\varepsilon_1+\varepsilon_2}(h/w)\right) \quad (1)$$

$$\beta = acr\tan\left(\frac{y_c}{x_c}\right) = acr\tan\left(\frac{\left(\frac{l'_1-l'_2}{2}\right)\cos(\theta)}{\left(\frac{l'_1+l'_2}{2}\right)\sin(\theta)}\right) = \arctan\left(\frac{l'_1-l'_2}{l'_1+l'_2}\right)\cot(\theta) = acr\tan\left(\frac{l'_1-l'_2}{l'_1+l'_2}(w/h)\right) = acr\tan\left(\frac{\varepsilon_1-\varepsilon_2}{2+\varepsilon_1+\varepsilon_2}(w/h)\right) \quad (2)$$

$$\gamma_{xy} = \alpha + \beta \quad (3)$$

$$\delta_{sh} = \gamma_{yx}\cdot h \quad (4)$$

3. Experimental results and discussion

3.1. General behavior and failure modes

Load-deflection curves were obtained after loading the beams under four-point bending tests. Although load-controlled testing was adopted for flexural tests, a sample displacement ramp was also provided in Fig. 6. Obtained load-deflection curves are shown

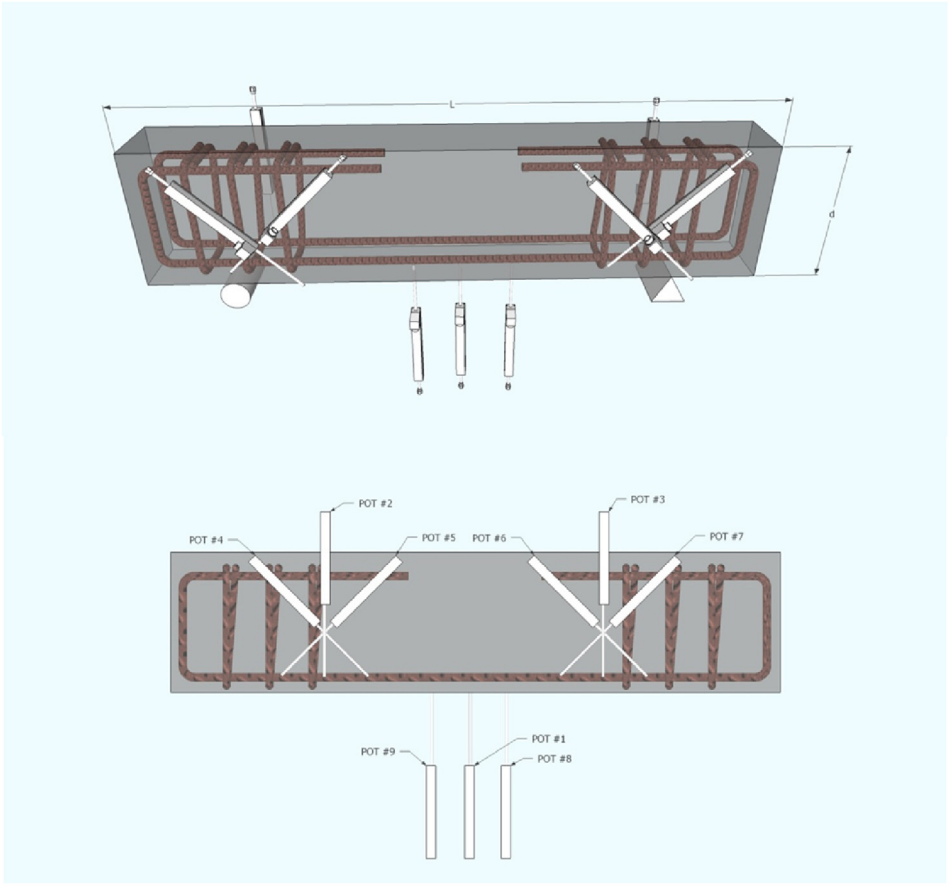

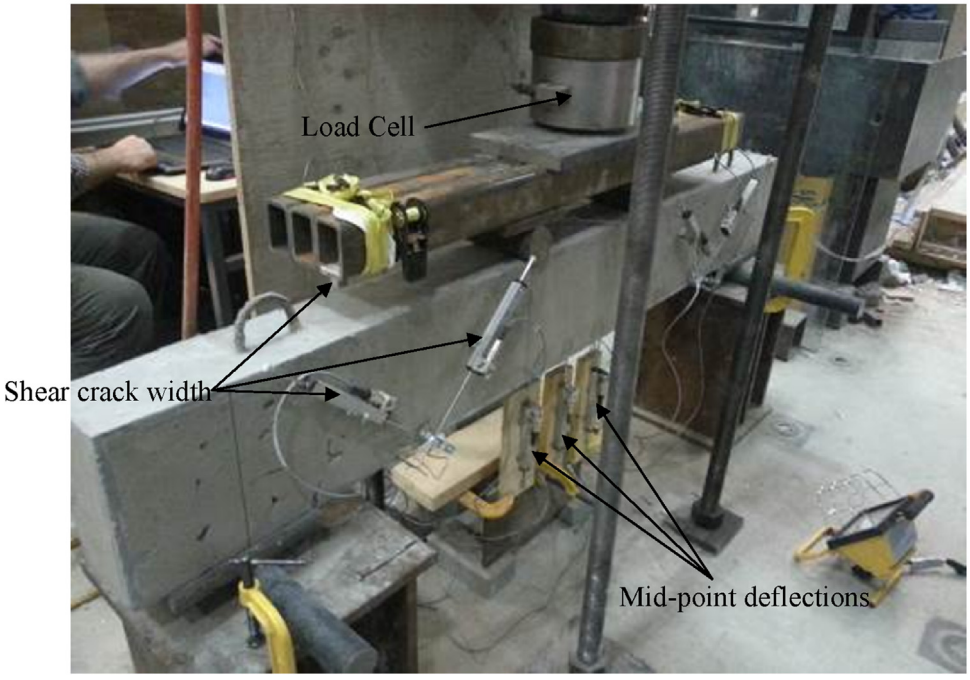

Fig. 4. Test setup and instrumentation.

in Fig. 7 for each test group. Each test group included beam specimens with four different a/d ratios. In the first group, beams were loaded up to failure after 28 days of standard curing. The second group beams were initially loaded up to 50% of their load-carrying capacity (as determined from the first group), and immediately after unloading, were reloaded up to failure at 28 days to assess the effect of pre-damage. Beams in the third group were used to evaluate the self-healing characteristics of reinforced ECC; at the age of

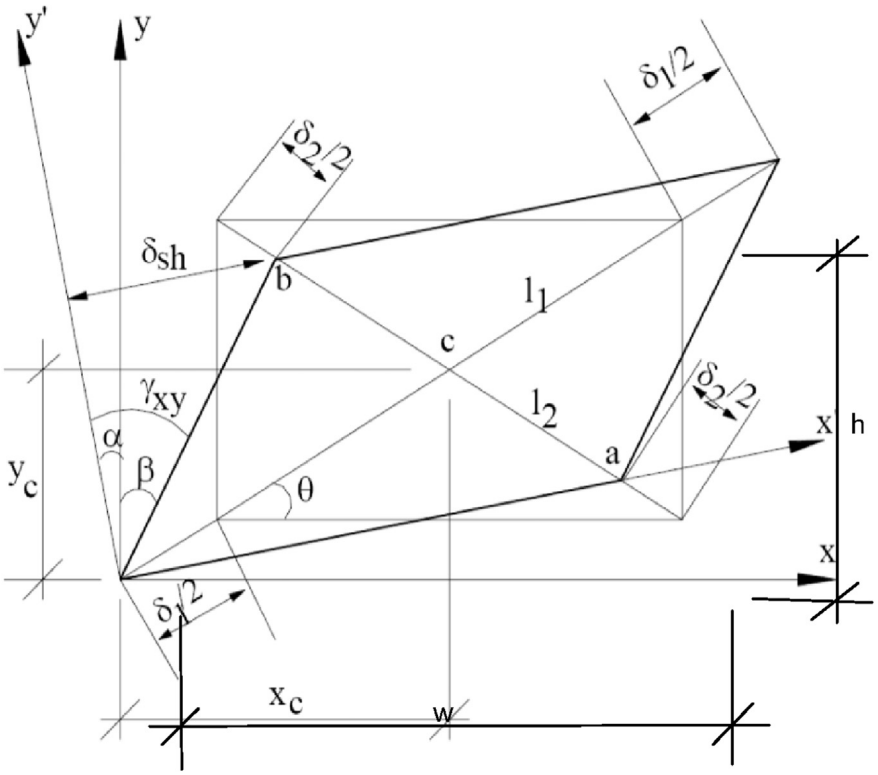

Fig. 5. Vertical shear deflection calculation approach for diagonal shear crack.

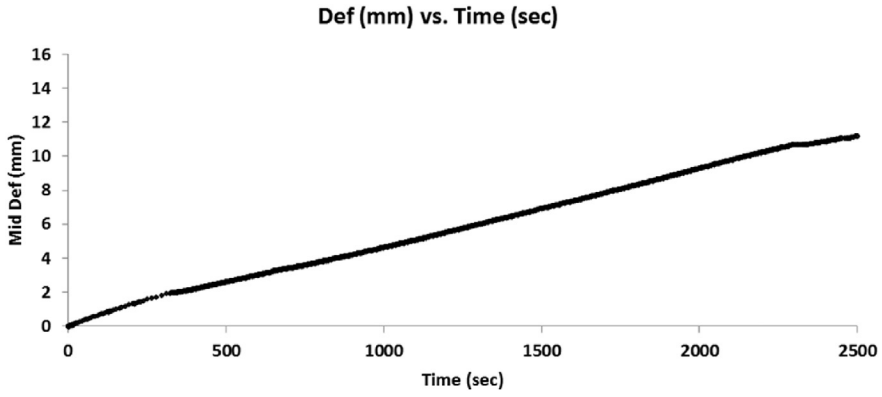

Fig. 6. Sample displacement ramp adopted for loading.

28 days, loads of up to 50% of the beams' load-carrying capacities were applied. After damage occurred, the load was removed. The pre-cracked beams were cured for an additional 30 days under wet burlap for self-healing. At the age of testing, beam specimens in the third group were tested until failure. For each test specimen, general behavior, failure mode, strength, stiffness, ductility and energy absorption capacity were determined from the load-deflection curves; the results are tabulated in Table 3. Examples of crack distribution and failure modes of specimens after testing are also shown in Fig. 8.

Beams from the first group were tested to determine the maximum load-carrying capacities of specimens with a/d ratios ranging between 1 and 4 at 28 days. Although the reinforced concrete beams produced with ECC did not have any shear reinforcement, most of the specimens showed flexural failure, and tensile reinforcement bars reached their yielding capacities. During loading for every beam specimen, cracks were initiated at the tension zone parallel to loading direction. As the load was increased, depending on the a/d ratio, diagonal cracks started to form close to the support points and propagated towards the loading point. Tensile reinforcements of beams 1, 2, 3 and 4 reached their yielding capacities under 403.60 kN, 211.45 kN, 120.96 kN and 86.43 kN load levels, respectively. As the a/d ratio increased, the beams reached the yielding point at a higher displacement level, while showing lower stiffness. For the beam specimens tested, reinforcement bars yielded at a load level of 81–97% of the ultimate load-carrying capacity. Additionally, with the exception of the a/d ratio of 2, all beam specimens exhibited flexural failure due to crushing of concrete in the compression zone. In the case of the a/d of 2, bending cracks initiated in the maximum moment zone. Then, as the load was increased, shear cracks formed in the right shear span. After the tensile reinforcement of the beam yielded, the

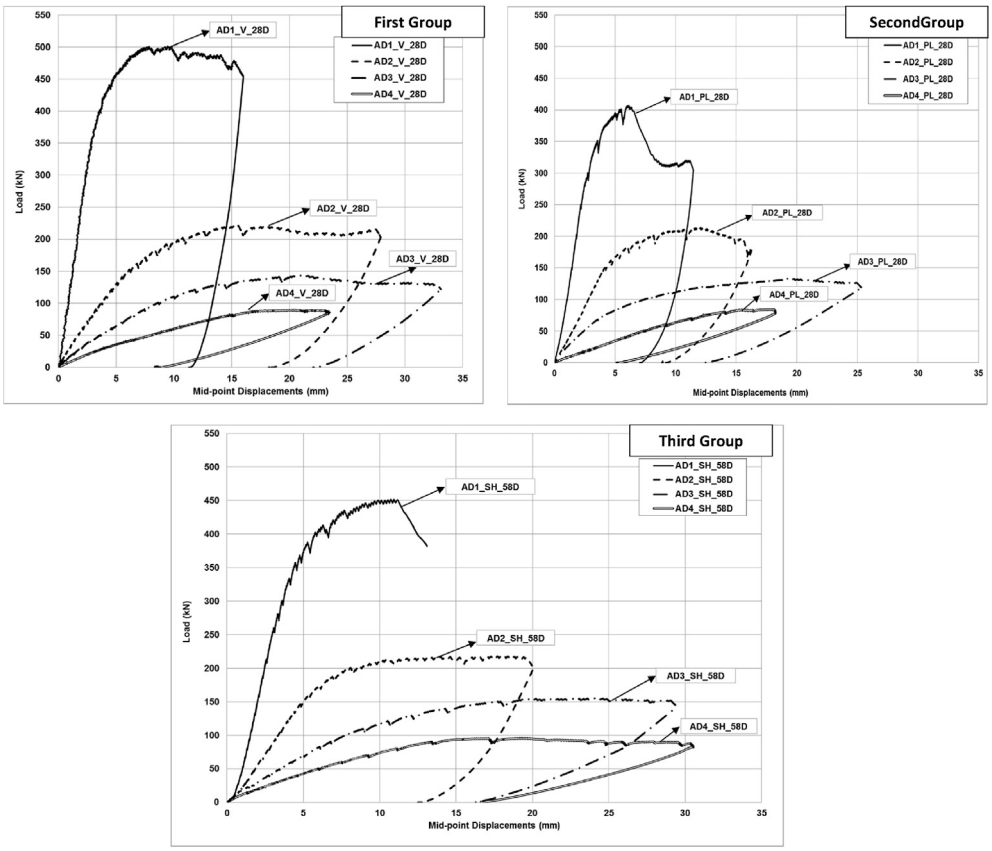

Fig. 7. Load-deflection curves of specimens.

Table 3
Overall results of beam specimens after four-point bending tests.

Spec. #	Concrete type/beam name	Load capacity (kN)		Deflection (mm)		Ductility ratio	Yield stiffness (kN/mm)	Energy absorption capacity (kN-mm)	Maximum strain at tension reinf. (με)	Failure mode
		Yield	Ultimate	At yield	At failure					
1	AD1_V_28D	403.60	501.47	3.71	16.01	4.32	108.79	6113	10021	Flexure
2	AD2_V_28D	211.45	220.66	12.58	27.36	2.18	16.81	4269	2536	Flexure-Shear
3	AD3_V_28D	120.96	143.27	11.79	32.75	2.78	10.26	3093	3983	Flexure
4	AD4_V_28D	86.43	89.43	16.69	23.40	1.40	5.18	945	12311	Flexure
5	AD1_PL_28D	371.14	406.91	3.50	11.45	3.27	106.04	3034	5988	Flexure
6	AD2_PL_28D	168.96	213.96	5.41	16.27	3.01	31.23	2203	8559	Flexure
7	AD3_PL_28D	102.18	131.98	7.77	25.34	3.26	13.15	2011	16082	Flexure
8	AD4_PL_28D	80.32	84.31	14.03	18.23	1.30	5.72	547	7113	Flexure
9	AD1_SH_58D	413.30	451.54	6.27	13.08	2.08	65.92	4310	16054	Flexure
10	AD2_SH_58D	200.10	217.49	10.06	20.06	1.99	19.89	2885	9187	Flexure
11	AD3_SH_58D	149.41	154.69	16.35	29.36	1.80	9.14	2851	13707	Flexure
12	AD4_SH_58D	91.43	95.76	17.28	30.53	1.77	5.29	1841	14954	Flexure

specimen failed in a combination of flexural-shear behavior as a result of the enlargement of a shear crack in the right shear span (Fig. 8(a)–(d)).

Beams from the second group were used to determine the effects of preloading on the behavior of test members. Beam specimens were pre-cracked at 28 days by loading up to 50% of their maximum load-carrying capacities. Sample load-deflection curves for the preloading stage are shown in Fig. 9. These curves show that as a/d ratio increased, deflection values at the maximum load state also increased. Upon removing the preload, all beam specimens experienced a permanent average plastic deflection of 1.37 mm, which indicates the success of the pre-damaging process. In addition, none of the beam reinforcement bars yielded during preloading. Since the reinforcing bars experienced loading under their elastic limit, the effect of pre-loading on reinforcing bars can be ignored. Average shear crack widths were measured as 0.32 mm and the mid-point displacement as a result of shear cracks was 0.49 mm. The preloaded beam specimens were loaded up to failure immediately after unloading. The tensile reinforcement bars achieved their yield capacities at 371.1 kN, 168.9 kN, 102.2 kN and 80.3 kN load levels for a/d 1, 2, 3 and 4, respectively. These values are far below those obtained for sound specimens tested in the first

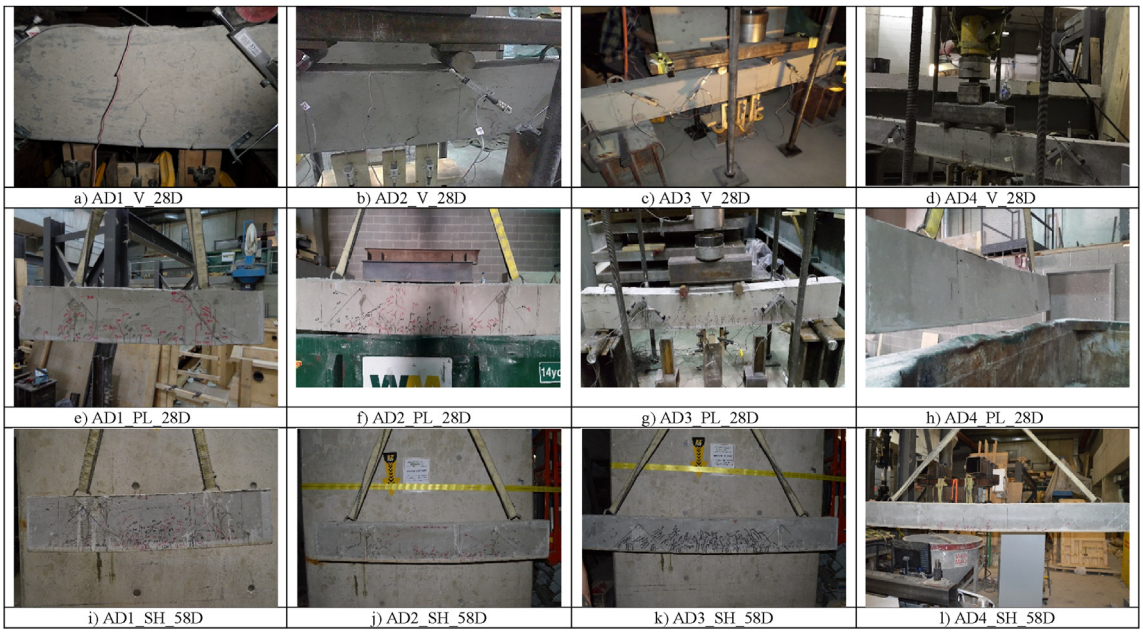

Fig. 8. Crack patterns of beam specimens after testing.

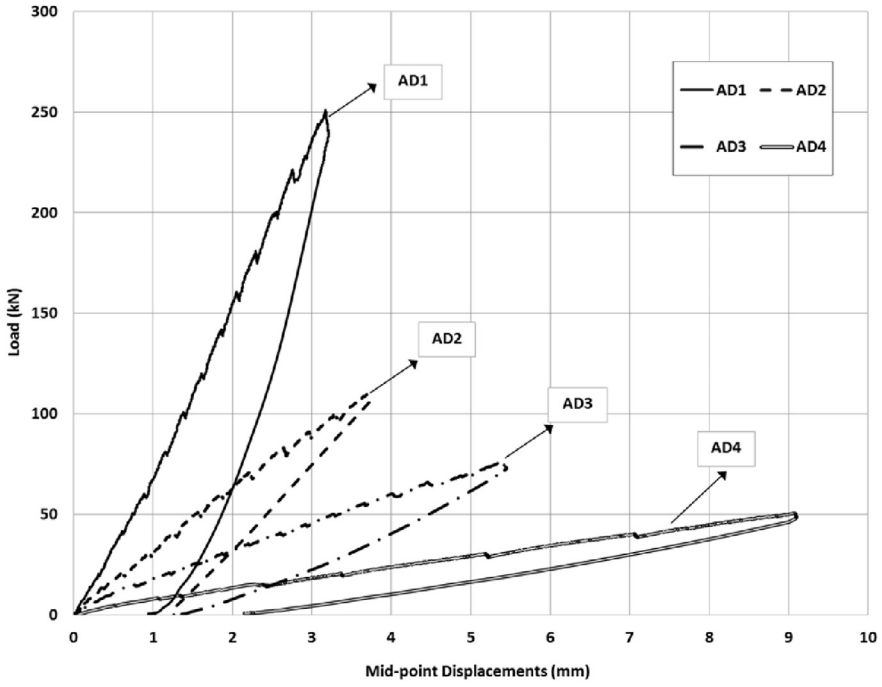

Fig. 9. Sample load-deflection graph of pre-loading of specimens at 28 days.

group. Like the sound beam specimens, yield points were reached at a higher load level as the a/d ratio increased with lower yield stiffness. For beam specimens reloaded up to failure, reinforcement bars yielded at a load level of 77–95% of the ultimate load-carrying capacity. (Fig. 8(e)–(h)).

Beam specimens in the third group were damaged by preloading up to 50% of their load-carrying capacities at 28 days, similar to the specimens in the second group. After unloading, they were cured with wet burlap for the standard curing period of 30 days (58 days total) to encourage self-healing. At 58 days, all beams were loaded up to failure. As seen from the load-deflection curves for the preloading stage presented in Fig. 9, the beam specimens showed an average of 5.37 mm mid-point displacement due to preloading and 1.38 mm permanent plastic mid-point displacement upon unloading. As the a/d ratio of the beam specimens increased, the mid-point deflection and permanent plastic deflection values increased as well. Shear crack widths increased up to an average of 0.37 mm at the maximum load, causing an average mid-point displacement of 0.51 mm. After self-healing, the tensile reinforcement of the beams yielded at 413.30 kN, 200.10 kN, 149.41 kN and 91.43 kN load levels for a/d 1, 2, 3, and 4, respectively, corresponding to 91.5–96.5% of the ultimate load-carrying capacities.

Without any change in the failure modes, self-healed beam specimens experienced similar performance in terms of load-carrying and deflection capacities to the sound specimens. All specimens showed flexural type of failure, except the beam with an a/d ratio of 2, which was loaded up to failure at 28 days and failed in a combination of shear and flexure. As a result, self-healing did not affect the failure type significantly.

3.2. Load capacity and stiffness

The yield stiffness and ultimate load-carrying capacity values of the beam specimens were determined from the load deflection curves provided in Fig. 7 and tabulated in Table 3. Besides the shear span to effective depth ratio of the beams, self-healing – the major variable investigated in the scope of the experimental study – was found to be effective on yield and ultimate load-carrying capacity of test specimens. Considering the a/d ratio, both the yield strength and maximum load-carrying capacity values of the test specimens decreased with the increase in the a/d ratio. When test specimens in the first group were loaded directly up to failure, yield strength values decreased 48, 70 and 79% witha/d values of 2, 3 and 4 from 1, respectively. Ultimate load-carrying capacity values also showed decreases of 56, 71 and 82% in the same manner. For the remaining test groups, yield and ultimate load-carrying capacities dropped with increased a/d in the same manner.

When specimens from the second group were loaded up to failure after subjected to preloading up to 50% of their ultimate load-carrying capacities, all yield and ultimate load-carrying capacity values decreased. Yield strength and maximum load-carrying capacities of the first group specimens were an average of 15% and 10% higher than those of the second test group. The second group specimens exhibited the lowest strength throughout the experimental program, which was mainly attributed to the applied preloading, which lowers their damage tolerance. For beams in the second group, those with an a/d ratio of 2 experienced the most dramatic decline in load-carrying capacity at yield. This behavior was attributed to the shear cracks that opened during preloading because shear cracks were denser than in the other beams. However the ultimate load-carrying capacity of this beam did not differ significantly. In spite of the small decline in ultimate load-carrying capacity, mid-span beam deflection values at both yield and failure almost halved. For the beam with an a/dratio of 1, shear cracks were also observed during preloading, although they were fewer in number. Preloading therefore did not affect load-carrying capacity at yield, but it significantly affected the ultimate load-carrying capacity and deflection at fracture. This difference between beams with a/d of 1 and 2 may be attributed to the fact that the yield and ultimate capacity of the beam with an a/d of 2 are too close to each other. Beams with an a/d ratio of 3 and 4 did not experience any shear cracking during preloading. The beam with a/d of 4 performed better in terms of load capacities and deflection values due to the limited number of finer cracks. It can be concluded that beams which experienced shear cracks during preloading also experienced greater decreases in their load and deflection capacities when they were loaded immediately up to failure after preloading. This may also be an outcome of the fact that shear cracks are significantly larger than bending cracks.

To evaluate the effect of self-healing on yield strength and maximum load-carrying capacity values, the results of the third group were compared with those of the other test groups. The third group specimens were initially damaged and subsequently subjected to the self-healing process. When the third group beams were compared to those of the first group in terms of yield strength, all third group specimens reached higher values with the exception of those with ana/d ratio of 2. This outcome indicates that the self-healing process was extremely successful and escalated yield strength to the level of sound specimens that were not pre-damaged. For specimens with an a/d ratio of 2, in which shear failure probability and damage was highest, yield strength was 5% lower. However, considering the devastating pre-damaging process that decreased yield capacity by around 20%, there was about a 15% improvement as a result of self-healing even though original yield strength could not be recovered. Similar results were obtained for maximum load-carrying capacity values, except for test specimens with an a/d ratio of 1; the maximum load-carrying capacity value for the third group was 10% lower than that of the first group. For the third group, specimens exhibiting flexural failure had a/d ratios of 3 and 4, with an average maximum load-carrying capacity 7.5% higher than that of the first test group specimens. Although all specimens exhibited flexural-type failure upon reloading after self-healing, the type of cracking (shear or bending) during preloading influenced self-healing performance in terms of load-carrying capacity. Specimens with a/d ratios of 3 and 4, which showed only bending cracks on preloading (almost no shear cracks were observed), performed better. This finding is extremely important since it reveals that the self-healing process leads to less satisfactory results on test specimens with intense shear damage than for those with more bending damage. When the yield strength and maximum load-carrying capacities of the specimens in the second group – which were tested after initial damage – were compared with third group specimens subjected to self-healing after initial damage, all a/d ratio capacities were an average of 22% and 11% higher for the third group specimens, respectively. These results point out the success of the self-healing process on healing damage and increasing strength. The best self-healing performance was observed for the beam with an a/d ratio of 3 in terms of yield and ultimate load-carrying capacities, when compared to the results of sound and preloaded specimens.

Stiffness of the tested beams was calculated where specimens reached their yielding points (Table 3). When the yield stiffness of the test specimens was investigated, they significantly dropped with the increase in a/d ratio for all test groups. For example, in the first group specimens, yield stiffness values decreased 85, 91 and 95% respectively when a/d ratio was gradually increased from 1 to 4. Decrement rates in stiffness values were 71, 88 and 95% in the second group, and 70, 86 and 92% for the third group. When evaluating self-healing, stiffness values can be used to confirm crack plugging with self-healing products, as stiffness is expected to drop due to preloading. During application of the load, pre-opened cracks would easily re-open at lower load levels. As they were plugged with self-healing products, stiffness was expected to increase again. However, due to the presence of reinforcement bars, yield stiffness may not adequately reflect the self-healing behavior. It can therefore be concluded that unlike small-scale plain ECC specimens, in large-scale reinforced ECC beams, yield stiffness is not sensitive to self-healing.

3.3. Ductility ratio

Ductility ratio is defined as the deflection at failure, normalized by that at yield point. The level where the load is dropped down to 85% of the ultimate load-carrying capacity was chosen as the failure point. The ductility ratios of all beam specimens are presented in Table 3. According to the results, they had a general tendency to decline as a/d ratios increased. The highest ductility ratios were achieved for beams with a/d ratios of 1 in every test groups. Although deflection at failure was the lowest for beams with an a/d ratio of 1, given the fact that the reinforcement bars yielded at a lower load and a lower deflection, the ductility ratio was the highest among all beams tested. Nonetheless, the lowest ductility

ratios were obtained in beam specimens with an a/d ratio of 4. For a/d ratios of 2 and 3, for the first and second groups, test beams with an a/d ratio of 2 showed lower ductility ratios. For the third group, beams with an a/d ratio of 3showed lower ductility ratios. However, ductility ratios were quite similar for all test groups for a/d ratios of 2 and 3. For the pre-damaged beams in the second test group, ductility ratios were higher for those with a/d ratios of 2 and 3 and lower for those with a/d ratios of 1and 4. Despite the fact that ductility ratio is expected to decline when the strength of regular concrete is decreased, the situation is quite different with reinforced ECC beams. Despite the fact that the pre-damaging process caused decreased deflection values at both yield and failure point, for beams that experienced escalation in ductility ratio after being pre-damaged, the main factor affecting the increase was the tremendous decrease in their deflection capacity at yield load. Because the pre-damaging process results in crack formation and decreases ECC strength, the increase in ductility ratio was unexpected. Unlike ordinary concrete, ECC has a deformation capacity of up to 300 times that of ordinary concrete, which is effective on the deformation behavior of reinforced ECC beams. The deflection capacity of beams (with an a/d ratio of 2) that suffered shear cracks on pre-loading decreased 57 and 41% at yield and failure, respectively. The second highest decrease in deflection values was 28% at failure, exhibited in the beam with an a/d ratio of 1. It can therefore be concluded that deflection capacity was also affected negatively by the shear cracks. Upon self-healing, all beam specimens experienced decreases in ductility ratio except those with an a/d ratio of 4. In addition, all deflection values (both at yield and failure) of the beams belonging to test group 3 improved, which was attributed to self-healing of previously opened cracks during pre-loading. At the same time, beams with a/d ratios of 3 and 4 recovered their ultimate deflection capacity the most. Among the self-healed beams, those with ana/d ratio of 3 showed only 10% lower deformation, while those with an a/d ratio of 4 showed a 30% increase over sound specimens tested at 28 days. These findings offer clear evidence of the success of the self-healing process, especially on beams with higher a/d ratios where pre-cracks formed only in the tensile zone.

3.4. Energy absorption capacity

Energy absorption capacities of the test beams were calculated as the area under load-deflection curves up to failure point. The failure points were assumed when the load dropped to 85% of the ultimate load-carrying capacity, as in the case of ductility ratio determination. The results for all test specimens are listed in Table 3. As the a/d ratio increased, energy absorption capacity decreased significantly in each test group. For example, in the control group (first group specimens), for a/d ratios of 1, 2, 3 and 4, the energy absorption capacities were 6113, 4269, 3093 and 945 kN-mm, respectively. The same declining trend was observed in the damaged (second group) and self-healed (third group) beam specimens.

A comparison of the energy absorption capacities of the first and second group test beams revealed that preloading up to 50% of maximum load-carrying capacity caused more than 40% reduction in energy absorption capacities for all a/d ratios. This was an expected result, as the crack formation in the damaged beams due to preloading increased brittleness. Due to preloading, both the load-carrying capacities and deformation amounts at failure decreased for all test beams, leading to a decrease in energy absorption capacities.

The third group test beams were preloaded up to 50% of their maximum load-carrying capacities and left for 30 days in a moist environment for self-healing to develop. At the end of 58 days, self-healed beams were reloaded up to failure. For all a/d ratios, self-healing increased the energy absorption capacities of beam specimens by at least 30% of the damaged beam results. The energy absorption capacities of the third group beam specimens were greater than those of second group according to each a/d ratio, which offers evidence of crack closure due to self-healing effect. The damaged test beams regained their ductility to some degree due to self-healing. Both the ultimate load-carrying capacities and deflections at failure increased for the self-healed beams, as discussed in the previous sections. These increments were reflected in the energy absorption results. Crack closure as a result of self-healing improved the properties of all beams tested.

When the energy absorption capacities of the first and third group test beams are compared, for a/d ratios of 1, 2 and 3, energy absorption capacities of control specimens tested at 28 days were greater than those of self-healed beams tested at 58 days. While the energy absorption capacities for a/d ratios of 1 and 2 were approximately 30% smaller in self-healed beams than in control specimens, the difference was approximately 8% for the a/d ratio of 3. Moreover, for the a/d ratio of 4, the energy absorption capacity of self-healed beams (1841 kN-mm) was much higher than in control specimens(945 kN-mm). The load-carrying capacity and deflection amount were also larger in self-healed beams with ana/d ratio of 4 than in the control beam. Beams cracked at 28 days with an a/d ratio of 4 showed crack closure, and the beam properties continued to develop during the additional 30 days of moist curing. The largest a/d ratio was chosen to promote a combination of shear and flexural failure. Self-healing appears to be more effective in flexural cracks when energy absorption capacity results are considered.

3.5. Measured tensile reinforcement strains

Table 3 illustrates the maximum strain values recorded for each beam, and Fig. 10 presents typical load-strain curves as an example. The yield strain of the steel bars used as tensile reinforcement in this study was 2549 με.

When the tensile reinforcement strains of the test specimens were examined, all specimens except the control beam with a/d ratio of 2 showed strain values that exceeded the strain limit for yielding. These findings are consistent with the failure mechanisms of the beam specimens. The control beam specimen with an a/d ratio of 2 showed a combination of flexural and shear failure mode. On the other hand, all other beams experienced flexural failure mode after reaching the yield capacity of their tensile reinforcement. Strain measurements of the tensile reinforcements are also compatible with the general load-deflection behaviors of the specimens.

The maximum strain values of tensile reinforcing steel bars were also employed to ensure that steel reinforcements in the second and third group beams did not yield during the preloading stage. Preloading up to 50% of maximum load-carrying capacities did not cause yielding of their tensile reinforcements.

3.6. Shear deflections

Diagonal shear deflections were determined by LVDTs placed symmetrically on both shear spans of the beams. The vertical components of the average diagonal shear deflections obtained at left and right shear spans were calculated according to the approach presented in Fig. 5. Vertical shear deflections, maximum mid-point deflections and the percentage of vertical shear deflections with respect to maximum mid-point deflections are provided in Table 4. Vertical shear deflections due to cracks occurred in shear spans, and their percentage to mid-span beam deflections provide valuable information about the shear behavior of beam

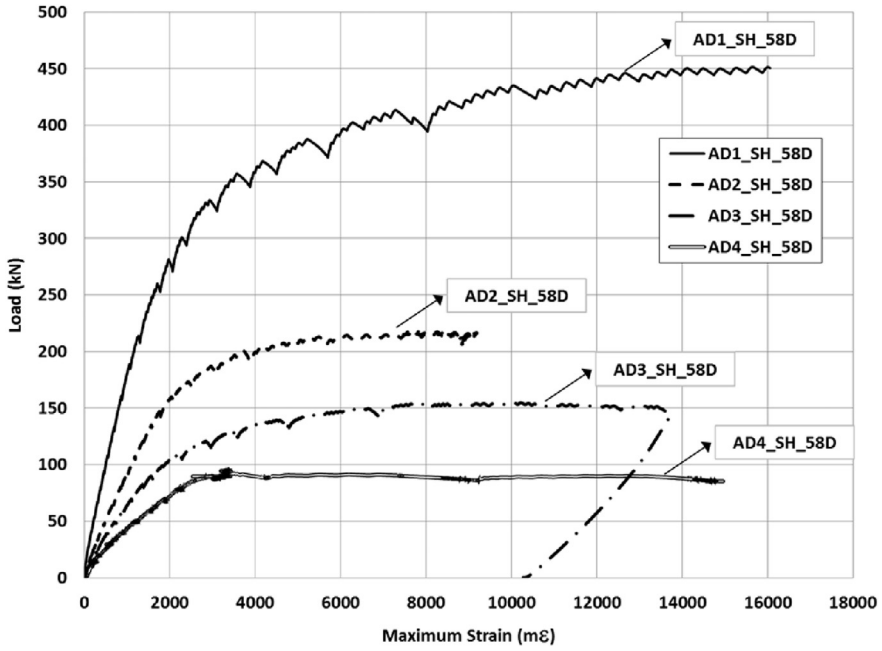

Fig. 10. Examples of load-strain graphs.

Table 4
Shear deflections of specimens.

Spec. #	Beam name	Mid-point deflection due to shear crack (mm)	Maximum mid-point deflection (mm)	Percentage[a] (%)
1	AD1_V_28D	0.44	16.01	2.75
2	AD2_V_28D	1.25	27.36	4.57
3	AD3_V_28D	0.66	32.75	2.02
4	AD4_V_28D	0.35	23.40	1.50
5	AD1_PL_28D	0.89	11.45	7.77
6	AD2_PL_28D	1.38	16.27	8.48
7	AD3_PL_28D	1.32	25.34	5.21
8	AD4_PL_28D	0.42	18.23	2.30
9	AD1_SH_58D	0.92	13.08	7.03
10	AD2_SH_58D	1.50	20.06	7.48
11	AD3_SH_58D	1.38	29.36	4.70
12	AD4_SH_58D	0.44	30.53	1.44

[a] Ratio of shear deflection to total mid-point deflection in percentage.

specimens. The higher the percentage of vertical shear deflection to maximum mid-span deflection, the higher the shear deflection, and hence a greater possibility of shear failure.

As seen in Table 4, the largest mid-point shear deflection and its percentage to mid-point deflection were obtained for an a/d ratio of 2 within each group. This is compatible with the fact that the sound beam with an a/d ratio of 2 was the only specimen that showed a combination of shear and flexural failure behavior (Table 3). When the results from the first and second group test beams were compared, it was observed that while vertical shear deflections increased, the total mid-point deflections decreased, leading to an increase in the percentage of shear deflection to mid-point deflection due to the application of preloading. Shear deflection percentages increased from 2.75, 4.57, 2.02 and 1.50% to 7.77, 8.48, 5.21 and 2.30%, respectively, due to preloading for a/d ratios of 1, 2, 3 and 4. Preloading up to 50% of maximum load-carrying capacity seemed to increase the possibility of brittle shear failure. In the third group, beams damaged at 28 days were left for self-healing for 30 days and tested at 58 days after casting. After the self-healing period, vertical deflections due to shear cracks were still higher than in the damaged beam results, regardless of a/d ratio. On the other hand, due to the self-healing maximum mid-point deflections were recovered to some degree for all a/d ratios. Shear deflection percentage to maximum deflection were 7.03, 7.48, 4.70 and 1.44% for a/d ratios of 1, 2, 3 and 4, respectively. Those deflection percentages decreased in self-healed beams compared to damaged beam specimens. Even though shear deflections did not decrease, the shear deflection percentages recovered as the result of self-healing. The preformed shear cracks reopened easily, most probably due to reloading. Moreover, in the case of a/d = 4, shear deflection percentages of self-healed beam specimens improved over sound beam specimens, indicating that the percentage was smaller than in the undamaged ones. These findings show that self-healing is not as effective on shear cracks as it is on flexural cracks. Shear deflection results support the fact that self-healing was less effective for specimens showing shear behavior, as also concluded for strength, ductility ratio and energy absorption capacity.

3.7. Visual inspection of cracks

The success of the self-healing process was also evaluated by visual inspection. Cracks formed during pre-loading were observed during re-loading after 30 days of curing for self-healing. To visually evaluate self-healing, pre-opened cracks were checked for evidence

of self-healing before the application of preloading. Most of the time, self-healing could be observed as a white deposit on the crack surfaces which is also observed for small scale ECC beams in the literature. This kind of white deposits are resulted by the reaction of Ca ions leaching from the hydration products and carbonates and/or carbonates produced as a result of the reaction of atmospheric CO_2 and water. Also $Ca(OH)_2$ may directly react with CO_2 to form $CaCO_3$ [7]. In general, tiny cracks – especially those close to the bottom of the beams – were almost healed in all specimens because bending cracks were narrower, making self-healing easier. It should be also considered that unlike other self-healing studies conducted in the literature, the self-healing processing this study was fostered by burlap wetted at regular intervals to evaluate the feasibility of self-healing in real-life situations. Another reason may be that gravity forced water to the bottom of the beams, decreasing the availability of water on the sides and making it easier for bending cracks to heal in comparison with shear cracks.

Propagation of cracks was observed during re-loading, which is another indicator of self-healing quality. Most of the pre-opened cracks that had self-healed did not re-open, especially bending cracks. Rather, it was observed that new cracks had begun to form from a different location. Even when existing cracks re-opened, they propagated at a greater load level than that used when they were formed during pre-loading. This is also a good indicator of the self-healing as it is known from the literature that formation of additional CSH gels as self-healing products in fly ash bearing ECC specimens due to the reaction of unhydrated fly ash particles with $Ca(OH)_2$ and water, yields in recovery in the mechanical properties rather than transport properties. The repeatability and pervasiveness of self-healing in ECC has already been revealed for small scale specimens for both containing fly ash and ground granulated blast furnace slag [25]. However, self-healing was not successful for shear cracks in comparison with bending cracks; only a small number of shear cracks close to the bottom face of the tested beams could be fully healed.

4. Conclusions

The study outlined in this paper investigated the effect of various shear span to effective depth ratios and the self-healing process on the performance of large-scale reinforced ECC beams. To interpret how important structural parameters changed with a/d ratios and especially with self-healing, general load-deflection behaviors, failure mechanisms, strengths, stiffnesses, ductility ratios, energy absorption capacities and shear displacements of three groups of specimens with four different shear span to effective depth ratios were compared. The conclusions are outlined below:

1) Large-scale reinforced ECC beams with four different a/d ratios were tested under four-point bending. Although no shear reinforcement was used in the production of the beam specimens, and more over the a/d ratios of the specimens were in the 1 to 4 range in which the risk of shear failure is more prominent, tensile reinforcements of all beam specimens reached their yield strength and specimens failed, exhibiting a ductile bending fracture, with the exception of those with an a/d ratio of 2.
2) With the increased a/d ratio (which is one of the variables examined in the scope of the study), substantial decreases in strength, stiffness and energy absorption capacity were observed.
3) The yield and maximum load-carrying capacities of specimens subjected to the self-healing process exceeded those of the specimens damaged prior to loading up to failure at the age of 28 days, with a/d ratios of 1–3. For instance the increases in yield strength were calculated as 11, 18 and 46% while for the ultimate load carrying capacities they were 11, 2 and 17% for a/d ratios of 1–3, respectively. All beam specimens enhanced their load carrying capacities as a result of self-healing process when compared to pre damaged beams. However they could not reach the level of sound beams. On the other hand, test specimens with an a/d ratio of 4, those subjected to self-healing after initial pre-loading achieved load-carrying capacities exceeding the values of control specimens by 6 and 7% for yield and ultimate load carrying capacities, respectively. Energy absorption capacity and vertical shear deflection percentage to maximum mid-point deflection were especially improved. This finding shows that the self-healing process is much more successful on test specimens with an a/d ratio of 4, in which the bending mode is more dominant and shear failure is unlikely. This conclusion indicates that bending cracks that are shorter and have less surface friction heal better than longer shear cracks with more surface friction.
4) Regardless of a/d ratio, preloading adversely affected all the properties of large-scale reinforced ECC beams. However, the properties were recovered as a result of self-healing in 30 days. Load-carrying capacities, deflections, energy absorption capacities and yield stiffness values of the damaged beam specimens were especially improved after self-healing.

The experimental work conducted in this study is intended to help us understand whether the intrinsic self-healing ability of ECC – which has been revealed in numerous studies for small-scale specimens – is valid for structural-size large-scale beams. The study shows that besides offering enhanced mechanical performance, the intrinsic self-healing ability of ECC can be taken advantage of for large-scale beams.

Acknowledgement

The authors gratefully acknowledge the financial assistance of the Scientific and Technical Research Council (TUBITAK) of Turkey provided under Project: MAG-112M876 and the Turkish Academy of Sciences, Young Scientist Award program. The second author would also like to acknowledge the financial support of TÜBITAK for the 2219 Scholarship.

References

[1] Yunovich M, Thompson NG. Corrosion of highway bridges: economic impact and control methodologies. Concr Int 2003;25:52–7.
[2] Bettigole NH. Rebuilding our bridges – why and how. ASTM Stand News 1994;22:24–7.
[3] Virmani YP, Clemena GG. Corrosion protection-concrete bridges. Report No. FHWA-RD-98–088. FHWA; Sept. 1998.
[4] Woudhuysen J, Abley I. Why is Construction so Backward. London: Wiley-Academy; 2004.
[5] Raupach M. Concrete repair according to the new European standard EN-1504. In: Alexander MG, Beushausen HD, Dehn F, Moyo P, editors. Proceedings of International conference on repair, rehabilitation and retrofitting; 2006. p. 6–8.
[6] Tang W, Kardani O, Cui H. Robust evaluation of self-healing efficiency in cementitious materials – a review. Constr Build Mater 2015;81:233–47.
[7] Yıldırım G, Kasap Keskin O, Keskin SB, Şahmaran M, Lachemi M. A review of intrinsic self-healing capability of engineered cementitious composites: recovery of transport and mechanical properties. Constr Build Mater 2015;101:10–21.
[8] Jacobsen S, Marchand J, Homain H. SEM observations of the microstructure of frost deteriorated and self-healed concrete. J Cem Concr Res 1995;25:1781–90.
[9] Reinhardt H, Joos M. Permeability and self-healing of cracked concrete as a function of temperature and crack width. J Cem Concr Res 2003;33:981–5.
[10] Sahmaran M, Yaman IO. Influence of transverse crack width on reinforcement corrosion initiation and propagation in mortar beams. Can J Civ Eng 2008;35:236–45.
[11] Edvardsen C. Water permeability and autogenous healing of cracks in concrete. ACI Mater J 1999;96:448–55.

[12] Aldea C, Song W, Popovics JS, Shah SP. Extent of healing of cracked normal strength concrete. J Mater Civ Eng 2000;12:92–6.
[13] Clear CA. The effects of autogenous healing upon the leakage of water through cracks in concrete. Wexham Springs: Cement and Concrete Association; 1985. p. 28.
[14] Tran Diep PT. Quasi-brittle self-healing materials: numerical modeling and applications in civil engineering. Ph.D. Thesis. National University of Singapore; 2011.
[15] Dry C. Repair and prevention of damage due to transverse shrinkage cracks inbridge decks. In: Liu S-C, editor. Proceedings of smart structures and materials; 1999. p. 253–6.
[16] Sahmaran M, Yildirim G, Erdem TK. Self-healing capability of cementitious composites incorporating different supplementary cementitious materials. Cem Concr Compos 2013;35:89–101.
[17] Barretta R, Luciano R. Exact solutions of isotropic viscoelastic functionally graded Kirchhoff plates. Compos Struct 2014;118:448–54.
[18] Barretta R, Luciano R. Analogies between Kirchhoff plates and functionally graded Saint-Venant beams under torsion. Continuum Mech Thermodyn 2015;27:499–505.
[19] Barretta R, Luciano R, Willis JR. On torsion of random composite beams. Compos Struct 2015;132:915–22.
[20] Barretta R, Luciano R, Marotti de Sciarra F. A fully gradient model for Euler-Bernoulli nanobeams. Math Problems Eng 2015;2015:1–8. http://dx.doi.org/10.1155/2015/495095. Article ID 495095.
[21] Barretta R, Feo L, Luciano R, Marotti de Sciarra F. Application of an enhanced version of the Eringen differential model to nanotechnology. Compos Part B 2016;96:274–80.
[22] Barretta R, Feo L, Luciano R, Marotti de Sciarra F. An Eringen-like model for Timoshenko nanobeams. Compos Struct 2016;139:104–10.
[23] MacGregor JG, Wight JK, Teng S, Irawan P. Reinforced concrete: mechanics and design. Upper Saddle River, NJ: Prentice Hall; 1997.
[24] Yang E, Sahmaran M, Yang Y, Li VC. Rheological control in the production of engineered cementitious composites. ACI Mater J 2009;106(4):357–66.
[25] Sahmaran M, Yildirim G, Noori R, Ozbay E, Lachemi M. Repeatability and pervasiveness of self-healing in engineered cementitious composites. ACI Mater J 2014;11:1–6.

Appendix

The following symbols are used in this paper

a: distance between applied shear force and support
d: effective depth (distance between upper concrete fiber and tensile reinforcement)
φ: diameter of tensile reinforcement
f_{sy}: yield strength of tensile reinforcement
f_{su}: ultimate strength of tensile reinforcement
E: elastic modulus of tensile reinforcement
θ: angle between the diagonal and horizontal axis in rectangular
h: height of the rectangular
w: width of the rectangular
l_1: length of first diagonal of rectangular
l_2: length of second diagonal of rectangular
l'_1: length of first diagonal of rectangular after deformation
l'_2: length of second diagonal of rectangular after deformation
ε_1: strain in the direction of first diagonal
ε_2: strain in the direction of second diagonal
δ_1: Deflection in the direction of first diagonal
δ_2: deflection in the direction of second diagonal
x_a: x coordinate of point A
y_a: y coordinate of point A
x_b: x coordinate of point B
y_b: y coordinate of point B
x_c: x coordinate of point C
y_c: y coordinate of point C
δ_{sh}: shear deflection